VIP-producing enteric neurons interact with innate lymphoid cells to regulate feeding-dependent intestinal epithelial barrier functions

Jhimmy Talbot[1], Paul Hahn[1], Lina Kroehling[1], Henry Nguyen[1], Dayi Li[1], & Dan R. Littman[1,2]

[1]Molecular Pathogenesis Program, The Kimmel Center for Biology and Medicine of the Skirball Institute, New York University School of Medicine, New York, NY 10016, USA

[2]Howard Hughes Medical Institute, New York, NY 10016, USA.

Correspondence: dan.littman@med.nyu.edu

ABSTRACT

The intestinal mucosa serves as both a conduit for uptake of food-derived nutrients and microbiome-derived metabolites and as a barrier that prevents tissue invasion by microbes and tempers inflammatory responses to the myriad contents of the lumen. How the intestine coordinates physiological and immune responses to food consumption to optimize nutrient uptake while maintaining barrier functions remains unclear. Here, we describe how a gut neuronal signal triggered by food intake is integrated with intestinal antimicrobial and metabolic responses controlled by type 3 innate lymphoid cells (ILC3)[1-3]. Food consumption rapidly activates a population of enteric neurons that express vasoactive intestinal peptide (VIP)[4]. Projections of VIP-producing enteric neurons (VIPen) in the lamina propria are in close proximity to clusters of ILC3 that selectively express VIP receptor type 2 (VIPR2 or VPAC2). ILC3 production of IL-22, which is up-regulated by commensal microbes such as segmented filamentous bacteria (SFB)[5-7], is inhibited upon engagement of VIPR2. As a consequence, there is a reduction in epithelial cell-derived antimicrobial peptide, but enhanced expression of lipid-binding proteins and transporters[8]. During food consumption, activation of VIPen thus enhances growth of epithelial-associated SFB and increases lipid absorption. Our results reveal a feeding- and circadian-regulated dynamic intestinal neuro-immune circuit that promotes a trade-off between innate immune protection and efficiency of nutrient absorption. As intestinal pathogenic microbes disrupt this neuro-immune inhibitory axis, targeting this pathway may enhance intestinal barrier function to prevent invasion by enteropathogens[2,3,9].

MAIN TEXT

Type 3 innate lymphoid cells (ILC3) promote maintenance of intestinal immune and metabolic homeostasis by integrating cytokine-mediated and glia-derived cues and, through the production of IL-22 and other cytokines, conveying information from the luminal microbiota to intestinal epithelial cells (IECs) and cells in the lamina propria [1-3,5,10]. The activation of ILC3 is regulated by cytokines, including IL-23, IL-1β, and TL1A, which are produced by mononuclear phagocytes and induced by intestinal microbe-derived stimuli[5,7,11]. Cytokines produced by activated ILC3, particularly IL-22, support the production of antimicrobial peptides (*e.g.* *RegIIIγ*) and mucin by IECs, ensuring spatial segregation of microbes from the intestinal tissue[12,13]. This microbiota-ILC3-IEC circuit promotes intestinal barrier function by controlling intestinal commensal microbiota and mediating rapid protective responses to enteropathogens[2,3,9,12]. Different subtypes of ILC3s are present within the intestinal lamina propria and are dispersed or in tertiary lymphoid tissue clusters known as cryptopatches (CPs) and isolated lymphoid follicles (ILFs)[14,15]. In perusing transcriptomic datasets of small intestinal ILCs, we noticed in CCR6^{+} ILC3, which comprise the lymphoid tissue inducer (LTi) cells enriched in CPs and ILFs, selective expression of multiple neurotransmitter/neuropeptide receptors and genes related to axonal guidance and neuron differentiation when compared to CCR6^{neg} ILC3 and NCR^{+} ILC3 (Fig. 1a and Extended Data Fig. 1a-c)[16,17]. This prompted us to evaluate whether CCR6^{+} ILC3 in the intestinal lamina propria were associated with neuronal projections from the enteric nervous system (ENS). The ENS is part of the peripheral autonomic nervous system, which controls gastrointestinal functions by

promoting rapid gut responses to changes in the luminal compartment (e.g. food intake, microbes, metabolites, etc.[18-22]). We observed that ILC3 in CPs/ILFs were in close proximity to neuronal projections in the lamina propria (Fig. 1b-d and Supplementary Videos 1,2). The CP/ILF-associated neuronal projections were positive for vasoactive intestinal peptide upon staining with specific antibody (VIP, Fig. 1e and Extended Data Fig. 2). We also observed association of VIPen and colonic lymphoid patches (Extended Data Fig. 3a,b). Indeed, ILC3 in CPs/ILFs were closer to VIP^+ enteric neurons (VIPen) than to neurons positive for substance P or tyrosine hydroxylase (which produce norepinephrine or dopamine) (Fig. 1f and Extended Data Fig. 2). These anatomical findings, together with the fact that $CCR6^+$ ILC3 express a high amount of VIP receptor type 2 (*Vipr2*) (Fig. 1a), prompted us to investigate whether signaling from VIPen could modulate $CCR6^+$ ILC3 functions and intestinal immune homeostasis.

We isolated ILC3 from the lamina propria of the small intestine of C57BL/6 mice (Extended Data Fig. 4a) and observed that *in vitro* activation of VIPR2 inhibited IL-23-induced production of IL-22 by $CCR6^+$ ILC3 (Fig. 2a,b and Extended Data Fig. 4b,c), although there was no effect on cell activation (marked by Sca-1 up-regulation) or on IL-22 production by $CCR6^{neg}$ ILC3 (Extended Data Fig. 4d-f). In order to investigate the *in vivo* role of VIPR2 activation in $CCR6^+$ ILC3 functions, we generated mixed bone marrow chimeric mice reconstituted with a 1:1 ratio of isotype-marked $Vipr2^{+/+}$ and $Vipr2^{-/-}$ cells. IL-22 was expressed in a greater proportion of $Vipr2^{-/-}$ $CCR6^+$ ILC3 when compared to $Vipr2^{+/+}$ ILC3 (Extended Data Fig 5a,b). We also generated mice with conditional deletion of the gene encoding VIPR2 in ILC3 ($Rorc(t)^{Cre}Vipr2^{fl/fl}$, or $ILC3^{\Delta Vipr2}$) and found that a larger proportion and number of $CCR6^+$ ILC3 isolated from the small

intestine of ILC3$^{\Delta Vipr2}$ mice expressed IL-22 than cells isolated from WT littermates (Fig. 2c and Extended Data Fig. 5c-f). Epithelial *RegIIIγ* mRNA, regulated by IL-22, was considerably higher in IECs from ILC3$^{\Delta Vipr2}$ mice when compared to WT mice (Fig. 2d), suggesting that VIPen-derived neuropeptide acts through VIPR2 to inhibit ILC3-mediated innate immune responses.

To determine whether direct modulation of VIPen (inhibition or activation) could affect ILC3 function, we adopted a chemogenetic strategy utilizing mice engineered to express designer receptors exclusively activated by designer drugs (DREADD)[23]. We selectively expressed inhibitory DREADD (hM4Di) in VIPen of *Vip*$^{IRES\text{-}Cre}$*hM4Di*$^{fl\text{-}stop\text{-}fl/+}$ mice and observed a higher frequency of IL-22-producing CCR6^{+}ILC3 at 24h following VIPen inhibition with the DREADD ligand clozapine-N-oxide (CNO, Fig. 2e,f). In parallel, there was increased *RegIIIγ* mRNA expression in the IECs after VIPen inhibition (Fig. 2g). Conversely, mice expressing the activating DREADD (hM3Dq) in VIPen (*Vip*$^{IRES\text{-}Cre}$*hM3Dq*$^{fl\text{-}stop\text{-}fl/+}$ mice) had fewer IL-22^{+} cells among the CCR6^{+} ILC3 and lower *RegIIIγ* mRNA in IECs following VIPen activation with CNO (Fig. 2h-j). Combined, these results indicate that VIPen modulates intestinal immune homeostasis, acting through VIPR2 on CCR6^{+} ILC3 to inhibit cell activation and IL-22 production.

We next investigated whether alteration of VIPen activity contributes to changes of intestinal barrier function during intestinal colonization with an enteropathogen. As previously described[24], following infection with *Citrobacter rodentium* there was increased *Vip* mRNA expression in the proximal colon and cecum and of VIP amounts in the portal vein, but not in the peripheral blood (Extended Data Fig. 6a-c), suggesting

an increase in VIPen activity in the intestinal tissue. Oral gavage of mice with a relatively low dose of *C. rodentium* ($2x10^9$ CFU) is tolerated by mice with an intact immune system. However, DREADD-mediated activation of VIPen during the first 4 days of infection led to increased bacterial translocation to the spleen and liver (Fig. 2k,l) and resulted in reduced survival (Fig. 2m), despite only a moderate increase in the amount of luminal *C. rodentium* (Extended Data Fig. 6d). Gavage with a high dose of *C. rodentium* ($4x10^{10}$ CFU) resulted in large amounts of bacteria that translocated to the liver and spleen (9d.p.i.) (Fig. 2n,o). DREADD-mediated inhibition of VIPen provided substantial protection from bacterial breach of the intestinal barrier without affecting the bacterial burden in the feces (Fig 2n,o and Extended Data Fig. 6e). Moreover, treatment with recombinant murine IL-22 reversed the effect of DREADD-mediated activation of VIPen on mortality and bacterial translocation (Extended Data Fig. 6f,g) Activation of VIPen during the events that follow infection with enteropathogens may therefore be an important contributor to intestinal barrier breakdown, which could be mitigated by inhibition of enteric VIP activity on ILC3.

These results suggested the existence of physiological signals that promote activation of VIPen during homeostasis, with consequent tonic inhibition of $CCR6^+$ ILC3. Food ingestion has been reported to rapidly signal VIP release in the intestine[4]. Indeed, we observed a greater amount of VIP in the ileum of mice sampled during the vivarium's dark-phase as compared to the light-phase, which correspond to periods of food consumption and resting, respectively (Extended Data Fig. 7a). Due to the *ad libitum* feeding scheme, approximately 15% of daily food intake occurs during the light-phase/resting period[25]. To dissect the effect of food intake on the VIPen immune

inhibitory axis and to reduce the noise created by feeding during the resting period, we restricted food availability for two weeks to alternating 12h cycles of feeding and fasting. To dissociate the effects of light/dark cycles from time of feeding, food was available to a group of mice only during the dark-phase (night-fed mice, ZT12-ZT0/6PM-6AM), while another group had food available only during the light-phase (day-fed mice, ZT0-ZT12/6AM-6PM). Using this scheme, we observed more VIP in the portal vein, but not in the peripheral blood, after 6h of food availability when compared to mice fasted for 6h, regardless of whether mice were fed during the light phase (ZT 6) or during the dark phase (ZT 18) (Extended Data Fig. 7b,c). In turn, the frequency of IL-22$^+$ CCR6$^+$ ILC3 was reduced during the periods of food consumption (at 6h of feeding) relative to fasting periods (fasted for 6 h), independently of light-dark cycles (Fig. 3a,b).

Using the mixed bone marrow chimeric mice, we observed among the *Vipr2*$^{+/+}$ CCR6$^+$ ILC3 a reduced frequency of IL-22$^+$ cells at 6h after start of food consumption (ZT 18) when compared to mice fasted for 6h (ZT 6) (Fig 3c and 3d). In contrast, there was no difference in frequency of IL-22$^+$ cells in the *Vipr2*$^{-/-}$ CCR6$^+$ ILC3 population with or without feeding. This is consistent with VIPR2 signaling-dependent inhibition of IL-22 production in CCR6$^+$ ILC3 following food intake. This conclusion was further supported by the observed reduction in the frequency of IL-22$^+$ CCR6$^+$ ILC3 at 6h following intragastric delivery of a liquid test diet, but not control saline, during the light-phase period (ZT1-ZT7) (Fig 3e,f). Furthermore, DREADD-mediated inhibition of VIPen abrogated the effect of the test diet on ILC3 (Fig. 3e and 3f). These results suggest a fast and dynamic temporal control of intestinal CCR6$^+$ ILC3 function promoted by food intake-mediated activation of VIPen and VIPR2.

Because IL-22 acts on intestinal epithelial cells to regulate barrier functions, including their interactions with commensal microbiota, we next examined whether the neuroimmune inhibitory circuit promoted by food consumption influences host-microbial interactions. There was elevated *RegIIIγ* mRNA expression in the IECs in mice fasted for 12h as compared to those fed during that time frame. In parallel, food consumption had a striking effect on the morphology of the ileal epithelium-associated segmented filamentous bacteria (SFB) (Fig. 4a-c and Extended Data Fig. 7d,e). SFB attached to IECs had long segmented filaments after 12h of food consumption, independently of light/dark cycles. However, in the ileum of mice fasted for 12h, independently of light-cycle, epithelium-associated SFB had few segments and were stubble-like. Short-term blockade with α-IL-22 reduced *RegIIIγ* mRNA expression in the IECs of mice during fasting, but not during feeding (Fig. 4c), and prevented control of SFB growth upon food restriction (Fig. 4d). In ILC3$^{\Delta Vipr2}$ mice, which have increased IL-22 production, SFB failed to form segmented filaments even after 12h of food consumption (Fig. 4e,f). These results suggest that VIPen regulate growth of the commensal microbiota by modulating cryptopatch-associated ILC3 in response to food consumption.

As IL-22 was recently shown to regulate lipid metabolism[8], at least in part by controlling genes involved in lipid transport, we examined the role of the VIPen-ILC3-IL-22 circuit in lipid absorption. Mice were adapted for 2 weeks to 12h restricted feeding during light or dark cycles and were then gavaged with ^{3}H-triolein following feeding or fasting. Mice that had been fed for 12h absorbed more of the triglyceride than mice fasted for 12h, although there was some effect of circadian regulation (light/dark adaptation) (Extended Data Fig. 7f,g). Expression of mRNAs for proteins associated

with fatty-acid/lipid uptake and transport (e.g. *Fabp2*) was lower in IECs from mice that were food-restricted for 12h compared to fed mice (Fig. 4g), in inverse relationship to *RegIIIγ* mRNA (Fig 4c). Moreover, short-term treatment with α-IL-22 during the fasting period reverted the expression of lipid transporters in IEC and ^{3}H-triolein absorption to amounts comparable to those observed with fed mice (Fig 4g,h).

The effect of food intake on IEC-dependent lipid absorption was dependent on VIPen inhibition of ILC3, since expression of lipid transporter mRNAs, ^{3}H-triolein absorption, and concentrations of circulating plasma triglycerides were substantially reduced in ILC3$^{\Delta Vipr2}$ when compared to WT mice after 12h of feeding (ZT 0) (Figures 4i-k). Finally, continuous intragastric delivery of a liquid test diet for 6h during the light phase period led to an increase in serum triglycerides, which was blocked by DREADD-mediated inhibition of VIPen (Fig. 4l).

These results reveal an important neuro-immune circuit in which feeding-activated VIPen antagonize microbiota-dependent CCR6^{+} ILC3 function, resulting in reduced IL-22 production and increased efficiency of lipid absorption. The benefit of greater nutrient acquisition comes at the expense of reduced barrier function, illustrated by susceptibility to enteropathic bacteria and rapid growth of epithelial-associated commensal SFB. Whether the host derives benefit from the reduced anti-microbial activity is unclear, although it may enable bacteria-dependent generation of essential metabolites[26] and vitamins that would be readily absorbed. Since enteric glial cells (EGCs) can secrete factors that act as activators of ILC3 functions[10], it will be important to determine how VIPen and EGCs coordinate antagonistic signals to promote efficient modulation of ILC3-mediated intestinal barrier functions, and also how neural development-associated

factors expressed by ILC3 (e.g. *Cntn1*, *Sema3d*, *Bmp2*) contribute to formation of neuro-immune cell units in cryptopatches/ILFs.

The mechanism by which the presence of food in the intestinal lumen is sensed and promotes VIPen activation is still unclear, and microbial[27,28], nutritional[4] or mechanical stimuli[29], acting peripherally or by way of the central nervous system, may be responsible for this. The VIP system has been implicated in circadian regulation centrally, as VIPR2 is required for expression of the core clock genes in the suprachiasmatic nuclei of the hypothalamus, and in the periphery, with circadian oscillation of IL-5 and IL-13 production by ILC2 and feeding-associated eosinophil recruitment in lung and gut mucosa[30,31]. While our study highlights the importance of food intake in regulating the VIPen, there is also a light-dependent contribution to the efficiency of lipid absorption, as there was only a partial effect when the feeding cycle was reversed. We therefore cannot rule out an additional role for central or peripheral clock functions independent of VIPen and ILC3.

Our results suggest that disturbances in feeding schedules could reduce intestinal barrier functions and promote dysbiosis and at the same time contribute to metabolic inbalance by chronic activation of VIPen. Moreover, enteropathogens may hijack this neuro-immune circuit and reduce intestinal barrier functions, facilitating intestinal colonization. In these scenarios, VIPR2 inhibitors may be valuable therapeutic tools to reduce lipid absorption or enforce the barrier during acute gastrointestinal infections.

Acknowledgements

We thank S.Y. Kim and the NYU Rodent Genetic Engineering Laboratory (RGEL) for generating the mutant mice. We also thank F-X. Liang, J. Sall, C. Petzold and K.

Dancel at the Microscopy Laboratory Core for timely preparation of the scanning electron microscopy images, and M. Cammer and Y. Deng for the help with optical microscopy. The Microscopy Core is partially supported by NYU Cancer Center Support Grant NIH/NCI P30CA016087, S10 RR023704-01A1 and NIH S10 ODO019974-01A1. This study benefitted from data assembled by the ImmGen Consortium. This work was supported by the Pew Latin American Fellows program (J.T.), the Helen and Martin Kimmel Center for Biology and Medicine (D.R.L.); and National Institutes of Health grant R01DK103358 (D.R.L.). D.R.L. is an Investigator of the Howard Hughes Medical Institute.

Author Contributions

J.T. and D.R.L. designed the study and analyzed the data. J.T. performed the experiments with assistance from P.H. and D.L., H.N. contributed to the feeding experiments, and L.K. performed the bioinformatics analyses. J.T. and D.R.L. wrote the manuscript. D.R.L. supervised the research.

FIGURE LEGENDS

Figure 1. Processes of VIP-producing enteric neurons are in close proximity to *Vipr2*-expressing ILC3 within cryptopatches. a, Heatmap of differentially expressed neural-related genes between intestinal CCR6^{+} ILC3 and CCR6^{neg} ILC3 (Fold change $\geq$ 2, *p-value <0.05,* GSE116092). Color scale is based on normalized read counts. Genes are listed on the right hand margin ranked based on the relative fold change, and color coded: Green: Neurotransmitter/neuropeptide receptors, Blue: genes related to nervous system

development/axonal guidance and contact. Expression in other ILC subsets is included for comparison. **b-d,** Representative confocal images from the small intestine of *Rorc(γt)*$^{EGFP/+}$ mice show clusters of intestinal ILC3 (cryptopatch) in close proximity to enteric neurons in the small intestine lamina propria (see supplementary video 1 and 2). Pan-neuronal marker: β3-tubulin^{+} (red), ILC3: GFP^{+}TCRβ^{neg} (green and blue, respectively). n=4 mice, 45 ILC3 clusters. **e, f,** Neurochemical code of cryptopatch-associated enteric neurons. (**e**) Representative confocal images from the small intestine of *Rorc(γt)*$^{EGFP/+}$ mice show cryptopatch-associated enteric neurons are positive for VIP. Neurons: β3-tubulin^{+} (red), VIP^{+} (green); ILC3: GFP^{+} (blue).

Figure 2. VIPen promote reduction of mucosal barrier function by VIPR2-dependent inhibition of CCR6^{+} ILC3. a, b, Representative FACS plot (**a**) and summaries (**b**) indicating IL-22 expression in purified CCR6^{+} ILC3 after *in vitro* IL-23 stimulation with/without VIPR2 agonist ligands. BAY: BAY-559837, VIP: vasoactive intestinal peptide. *P<0.05 and ***P<0.001 (*t-test*). Data are representative of three independent experiments. **c,** Number of IL-22^{+} CCR6^{+} ILC3 present in the ileum of *Rorc*^{Cre} (WT) and *Rorc*^{Cre} *Vipr2*$^{fl/fl}$(ILC3$^{\Delta Vipr2}$).. **P<0.01 (*t-test*), WT: 8; ILC3$^{\Delta Vipr2}$: 6. **d,** Normalized epithelial *Reg3γ* mRNA from ileum of WT and ILC3$^{\Delta Vipr2}$ mice. ***P<0.001 (*t-test*), WT: 5; ILC3$^{\Delta Vipr2}$: 5. **e-g,** Effect of VIPen inhibition on ILC3 and intestinal epithelial cells (IEC). Representative FACS plot (**e**) and summary (**f**) indicating IL-22 expression in CCR6^{+} ILC3 from the ileum of *Vip*$^{IRES\text{-}Cre}$ *hM4Di*$^{fl\text{-}stop\text{-}fl/+}$ mice (DREADD for VIPen

inhibition) 24h following treatment with vehicle or CNO (Clozapine-N-oxide, DREADD ligand). Vehicle: n=5, CNO: n=5. **P<0.01 (*t-test*). Data representative of three independent experiments. **g,** Normalized *Reg3γ* mRNA expression in IEC at 24h following treatment. Vehicle: n=3, CNO: n=3. *P<0.05 (*t-test*). Data representative of two independent experiments. **h-j,** Effect of VIPen activation on ILC3 and IEC. Representative FACS plot (**h**) and summaries (**i**) indicating IL-22 expression in $CCR6^{+}$ ILC3 from ileum of $Vip^{IRES\text{-}Cre}hM3Dq^{fl\text{-}stop\text{-}fl/+}$ (DREADD for VIPen activation) 24h following the treatment with vehicle or CNO. Vehicle: 6, CNO: 7. **P<0.01 (*t-test*). **j,** Normalized epithelial *Reg3γ* mRNA at 24h following treatment with vehicle or CNO. Vehicle: 7, CNO: 6. *P<0.05 (*t-test*). Data representative of three independent experiments. **k, l,** Dissemination of *C. rodentium* to the (**k**) spleen and (**l**) liver in $Vip^{IRES\text{-}Cre}hM3Dq^{fl\text{-}stop\text{-}fl/+}$ mice treated with vehicle or CNO (1mg/Kg, daily) for 4 days post-intragastric infection with $2x10^{9}$ CFU. Log_{10} Colony Forming Units (CFU) of *C. rodentium* 9 days post-oral innoculation (9 d.p.i.). Dotted line: limit of detection. ***P=0.0009 and ****P<0.0001, (*Mann-Whitney test*). Vehicle: n=11 (Positive for *C. rodentium:* spleen: 6/11, liver: 8/11), CNO: n=9 (Positive for *C. rodentium:* spleen and liver: 9/9). Data representative of two independent experiments. **m,** Survival rates for *C. rodentium*-infected $Vip^{IRES\text{-}Cre}hM3Dq^{fl\text{-}stop\text{-}fl/+}$ mice treated with vehicle or CNO (1mg/Kg, daily, 1-4 d.p.i.: blue rectangle). Vehicle: n=11, CNO: n=11. Data representative of three independent experiments. ****P<0.0001 *(Mantel-Cox test*). **n, o,** Bacterial dissemination to the (**n**) spleen and (**o**) liver of $Vip^{IRES\text{-}Cre}hM4Di^{fl\text{-}stop\text{-}fl/+}$ mice treated with vehicle or CNO (1mg/Kg, daily, 1-4 days post-intragastric infection with $4x10^{10}$ CFU of *C.*

rodentium). Log_{10} CFU at 9 d.p.i. Dotted line: limit of detection. Vehicle: n=8 (Positive for *C. rodentium:* spleen: 8/8, liver: 8/8), CNO: n=7 (Positive for *C. rodentium:* spleen: 1/7, liver: 1/7). ***P=0.0006 (spleen) and ***P=0.0005 (liver) (*Mann-Whitney test*)**.** Data representative of two independent experiments.

Figure 3. Feeding reduces IL-22 production by CCR6^{+}ILC3 through activation of VIPen. **a, b,** Representative FACS plot (**a**) and summaries (**b**) indicating IL-22 expression among CCR6^{+} ILC3 from the ileum of mice 6h after feeding or fasting, at ZT6 and ZT18. N=5, *P<0.05 (*t-test*). Data are representative of two independent experiments. **c,** IL-22 expression by CCR6^{+} ILC3 from the ileum of CD45.1 *Vipr2*$^{+/+}$:CD45.2 *Vipr2*$^{-/-}$ bone marrow chimeric mice 6h after fasting (fasted, ZT 6) and 6h after feeding (fed, ZT 18). n=7, *P<0.05 (*paired t-test*). Data are representative of two independent experiments. **d,** Ratio of IL-22-expressing cells, relative to Figure 3c, among CCR6^{+} ILC3 from the ileum of CD45.1 *Vipr2*$^{+/+}$:CD45.2 *Vipr2*$^{-/-}$ bone marrow chimeric mice 6h after fasting (Fasted, ZT 6) and 6 hours after feeding (Fed, ZT 18). n=7, *P<0.05 (*t-test*). **e, f,** Representative FACS plot (**e**) and summaries (**f**) indicating IL-22 expression in CCR6^{+} ILC3 from the ileum of *Vip*$^{IRES\text{-}Cre}$*hM4Di*$^{fl\text{-}stop\text{-}fl/+}$ mice (DREADD for VIPen inhibition). Mice were treated with vehicle or CNO (1mg/Kg) and 30 minutes later were fed by intragastric administration of saline (0.4 mL each 45 min, for 6 h) or Liquid Test Diet (500 mg/mL, 0.4mL each 45 minutes, for 6 h). N=4, **P<0.01 (*t-test*).

Figure 4. Dynamic regulation of commensal bacterial growth and lipid absorption by feeding-dependent VIP production . a, b, Representative scanning electron microscopy (SEM) images (**a**) of epithelium-associated commensal SFB in the

ileum of mice 12h after fasting or feeding at the end of the dark-phase (ZT 0) and the light-phase (ZT 12) and (**b**) measurements of SFB filament lengths. N=3, ****P<0.001 (*t-test*). **c,** Normalized epithelial *Reg3*γ mRNA expression in the ileum of mice treated with IgG or α-IL-22 (10mg/Kg) during the feeding period (Fed for 12h: Treated from ZT 12->ZT 0) or during the fasting period (Fasted for 12h: Treated from ZT 0->ZT 12). Data pooled from 2 independent experiments: Fed IgG1: N=8, Fed α-IL-22: N=8, Fast IgG1: N=8, Fed α-IL-22: N=7, *P<0.05 and **P<0.01 (*t-test*). **d,** SFB length in the ileum of mice treated with IgG or α-IL-22 (10mg/Kg) during the feeding period (Fed for 12h: ZT 12->ZT 0) or during the fasting period (Fast for 12h: ZT 0->ZT 12). N= 3, ****P<0.001 (*t-test*). **e,f,** Representative **(e)** SEM images of epithelium-associated SFB in the ileum of WT and ILC3$^{\Delta Vipr2}$ mice fed for 12h and **(f)** measurement of bacterial filament lengths. N= 3, ****P<0.001 (*t-test*). **g,** Normalized epithelial mRNA expression of *Fabp2* in the ileum of mice treated with IgG or α-IL-22 (10mg/Kg) during the fasting period (Fasted for 12h: Treated from ZT 0->ZT 12). Data pooled from 2 independent experiments: Fed IgG1: N=8, Fed α-IL-22: N=8, Fast IgG1: N=8, Fed α-IL-22: N=7. *P<0.05 and **P<0.01 (*t-test*). **h,** Plasma ^{3}H CPM (counts per minute) in 12h fasted mice after gavage with ^{3}H-triolein (1uCi/mice in 200ul of 20% Intralipid). Mice were treated with IgG or α-IL-22 (10mg/Kg) during the fasting period (Fasted for 12h: Treated from ZT 0->ZT 12). Data representative of 2 independent experiments. N=4, ***P<0.001 (*two-way ANOVA*). **i, j,** Normalized epithelial mRNA expression of *Fabp2* and *Cd36* (**i**) and plasma triglyceride content (**j**) in 12h fed WT (N=5) and ILC3$^{\Delta Vipr2}$ (N=4) mice**.** *P<0.05 and **P<0.01 (*t-*

335 *test*). **k,** Plasma ^{3}H CPM in 12h fed WT (N=3) and ILC3$^{\Delta Vipr2}$ (N=3) mice after gavage

336 with ^{3}H-triolein. ***P<0.001, (*two-way ANOVA*). **l,** Plasma triglyceride content in *Vip*$^{IRES-Cre}$*hM4Di*$^{fl\text{-}stop\text{-}fl/+}$ mice (DREADD for VIPen inhibition) after gavage with Saline (0.4

337

338 mL/each 45 minutes, for 6 hours) or Liquid Test Diet (500 mg/mL, 0.4mL/each 45

339 minutes, for 6 hours). Vehicle: N=5, CNO: N=4. **P<0.01, (*t-test*).

340

341

REFERENCES

1. Constantinides MG. Interactions between the microbiota and innate and innate-like lymphocytes. *J Leukoc Biol.* 2018;103(3):409-419.
2. Sonnenberg GF. Regulation of intestinal health and disease by innate lymphoid cells. *Int Immunol.* 2014;26(9):501-507.
3. Spits H, Cupedo T. Innate lymphoid cells: emerging insights in development, lineage relationships, and function. *Annu Rev Immunol.* 2012;30:647-675.
4. Chayvialle JA, Miyata M, Rayford PL, Thompson JC. Effects of test meal, intragastric nutrients, and intraduodenal bile on plasma concentrations of immunoreactive somatostatin and vasoactive intestinal peptide in dogs. *Gastroenterology.* 1980;79(5 Pt 1):844-852.
5. Sano T, Huang W, Hall JA, et al. An IL-23R/IL-22 Circuit Regulates Epithelial Serum Amyloid A to Promote Local Effector Th17 Responses. *Cell.* 2015;163(2):381-393.
6. Savage AK, Liang HE, Locksley RM. The Development of Steady-State Activation Hubs between Adult LTi ILC3s and Primed Macrophages in Small Intestine. *J Immunol.* 2017;199(5):1912-1922.
7. Longman RS, Diehl GE, Victorio DA, et al. CX(3)CR1(+) mononuclear phagocytes support colitis-associated innate lymphoid cell production of IL-22. *J Exp Med.* 2014;211(8):1571-1583.
8. Mao K, Baptista AP, Tamoutounour S, et al. Innate and adaptive lymphocytes sequentially shape the gut microbiota and lipid metabolism. *Nature.* 2018;554(7691):255-259.
9. Zheng Y, Valdez PA, Danilenko DM, et al. Interleukin-22 mediates early host defense against attaching and effacing bacterial pathogens. *Nat Med.* 2008;14(3):282-289.
10. Ibiza S, Garcia-Cassani B, Ribeiro H, et al. Glial-cell-derived neuroregulators control type 3 innate lymphoid cells and gut defence. *Nature.* 2016;535(7612):440-443.
11. Mortha A, Chudnovskiy A, Hashimoto D, et al. Microbiota-dependent crosstalk between macrophages and ILC3 promotes intestinal homeostasis. *Science.* 2014;343(6178):1249288.
12. Hooper LV, Littman DR, Macpherson AJ. Interactions between the microbiota and the immune system. *Science.* 2012;336(6086):1268-1273.
13. Dudakov JA, Hanash AM, van den Brink MR. Interleukin-22: immunobiology and pathology. *Annu Rev Immunol.* 2015;33:747-785.
14. Eberl G, Marmon S, Sunshine MJ, Rennert PD, Choi Y, Littman DR. An essential function for the nuclear receptor RORgamma(t) in the generation of fetal lymphoid tissue inducer cells. *Nat Immunol.* 2004;5(1):64-73.
15. Gury-BenAri M, Thaiss CA, Serafini N, et al. The Spectrum and Regulatory Landscape of Intestinal Innate Lymphoid Cells Are Shaped by the Microbiome. *Cell.* 2016;166(5):1231-1246 e1213.
16. Pokrovskii M, Hall JA, Ochayon DE, et al. Characterization of Transcriptional Regulatory Networks that Promote and Restrict Identities and Functions of Intestinal Innate Lymphoid Cells. *Immunity.* 2019.

17. Heng TS, Painter MW, Immunological Genome Project C. The Immunological Genome Project: networks of gene expression in immune cells. *Nat Immunol.* 2008;9(10):1091-1094.
18. Furness JB. The enteric nervous system and neurogastroenterology. *Nat Rev Gastroenterol Hepatol.* 2012;9(5):286-294.
19. Muller PA, Koscso B, Rajani GM, et al. Crosstalk between muscularis macrophages and enteric neurons regulates gastrointestinal motility. *Cell.* 2014;158(2):300-313.
20. Cardoso V, Chesne J, Ribeiro H, et al. Neuronal regulation of type 2 innate lymphoid cells via neuromedin U. *Nature.* 2017;549(7671):277-281.
21. Klose CSN, Mahlakoiv T, Moeller JB, et al. The neuropeptide neuromedin U stimulates innate lymphoid cells and type 2 inflammation. *Nature.* 2017;549(7671):282-286.
22. Margolis KG, Gershon MD. Enteric Neuronal Regulation of Intestinal Inflammation. *Trends Neurosci.* 2016;39(9):614-624.
23. Roth BL. DREADDs for Neuroscientists. *Neuron.* 2016;89(4):683-694.
24. Conlin VS, Wu X, Nguyen C, et al. Vasoactive intestinal peptide ameliorates intestinal barrier disruption associated with Citrobacter rodentium-induced colitis. *Am J Physiol Gastrointest Liver Physiol.* 2009;297(4):G735-750.
25. Kohsaka A, Laposky AD, Ramsey KM, et al. High-fat diet disrupts behavioral and molecular circadian rhythms in mice. *Cell Metab.* 2007;6(5):414-421.
26. Smith PM, Howitt MR, Panikov N, et al. The microbial metabolites, short-chain fatty acids, regulate colonic Treg cell homeostasis. *Science.* 2013;341(6145):569-573.
27. McVey Neufeld KA, Perez-Burgos A, Mao YK, Bienenstock J, Kunze WA. The gut microbiome restores intrinsic and extrinsic nerve function in germ-free mice accompanied by changes in calbindin. *Neurogastroenterol Motil.* 2015;27(5):627-636.
28. McVey Neufeld KA, Mao YK, Bienenstock J, Foster JA, Kunze WA. The microbiome is essential for normal gut intrinsic primary afferent neuron excitability in the mouse. *Neurogastroenterol Motil.* 2013;25(2):183-e188.
29. Chayvialle JA, Miyata M, Rayford PL, Thompson JC. Release of vasoactive intestinal peptide by distention of the proximal stomach in dogs. *Gut.* 1980;21(9):745-749.
30. Harmar AJ, Marston HM, Shen S, et al. The VPAC(2) receptor is essential for circadian function in the mouse suprachiasmatic nuclei. *Cell.* 2002;109(4):497-508.
31. Nussbaum JC, Van Dyken SJ, von Moltke J, et al. Type 2 innate lymphoid cells control eosinophil homeostasis. *Nature.* 2013;502(7470):245-248.

METHODS

Mice

C57Bl/6 mice were obtained from Taconic Farm. All transgenic mice were bred and maintained in the animal facility of the Skirball Institute (New York University School of Medicine) in specific pathogen-free conditions. *hM3Dq*$^{fl\text{-}stop\text{-}fl}$ mice (CAG-LSL-Gq-DREADD, Jax #026220), *hM4Di*$^{fl\text{-}stop\text{-}fl}$mice (CAG-LSL-Gi-DREADD, Jax #026219), *VIP*$^{IRES\text{-}Cre}$ mice (B6J.Vip-IRES-Cre, Jax #031628) and CD45.1 mice (*B6.SJL-Ptprca Pepcb/BoyJ*, Jax# 002014) were purchased from Jackson Laboratories. *Rorc*(γt)$^{EGFP/+}$ and *Rorc*^{Cre} mice were generated in our laboratory and previously described[14,22]. *Vipr2*$^{-/-}$ mice (Jax# 031332) were purchased from Jackson Laboratories and were maintained in a CD45.2 background or were bred with CD45.1 (*B6.SJL-Ptprca Pepcb/BoyJ*) mice, which subsequently generated *Vipr2*$^{-/-}$ CD45.1/2 mice and WT CD45.1 littermates. Conditional VIPR2 knockout (*Vipr2*$^{fl/fl}$) mice were generated using CRISPR-Cas9 technology as described below. Mice in all experiments were 6–12 weeks old at the starting point of treatments and all were colonized with SFB. All animal procedures were performed in accordance with protocols approved by the Institutional Animal Care and Usage Committee of New York University School of Medicine or the NIAID as applicable.

Generation of ILC3$^{\Delta Vipr2}$ *mice*

Mice carrying *loxP* sites flanking exons 3 and 4 of the Vipr2 gene (*Vipr2*$^{fl/fl}$) were generated using published CRISPR/Cas9 protocols[32,33] at the NYU School of Medicine's Rodent Genetic Engineering Laboratory. Briefly, guide RNAs targeting regions upstream of exon 3 (gRNA_16

sequence: GAAATCTCACAACAGATTCG) and downstream of exon 4 (gRNA_23 sequence: TCTCCTCAGAAGCATCGAAT) were designed using the Crispr guide design software (http://crispr.mit.edu/). gRNA recognition sequences were cloned into the pX330 vector (a gift from Dr. Feng Zhang, Addgene #42230), using oligos with a T7 promoter containing the gRNA template that were chemically synthetized by IDT (Integrated DNA Technologies). The products of PCR-amplified T7-gRNA were used as templates for in vitro transcription (MEGAshortscript T7 kit, Thermo Fisher Scientific). The gRNAs were purified using the MEGAClear Transcription Clean-up kit (Thermo Fisher Scientific). Two donor templates (ssDNA_1 and ssDNA_2) with 200bp each were chemically synthetized by IDT. The donor templates contained 60bp homology arms flanking a cassete containing a loxP sequence and XhoI or SalI restriction sites, located in the original PAM sequence (mutated PAM). Namely, ssDNA_1 (XhoI) for the region upstream exon 3: (GGATGGCATTTACATAGGACCCCATCCCAGTGGCTGCTCAGAAGAGCACTCACTCCTTA TCCctcgagataacttcgtataatgtatgctatacgaagttatCCGAATCTGTTGTGAGATTTCGAGAACTCATA AGGACTGATAAGGCCACACAACTTGAGC), and ssDNA_2 for the region downstream exon 4 (TGATTTCTCCTAGGTCACACTCAGGGAGCATTTCCAGACACTGGAAAACTCCTGAGGCC CgtcgacataacttcgtataatgtatgctatacgaagttatATTCGATGCTTCTGAGGAGACTATAATTAAACCC TGCCTGTGTGAGGCATGGCTTCTGAT). Mice were generated by injection of a mixture of mammalian optimized Cas9 mRNA (100 ng/µl, TriLink Biotechnologies), purified gRNA_16 and gRNA_23 (50 ng/µl, each) and donor templates ssDNA_1 and ssDNA_2 (50ng/ul, each) in injection buffer (10 mM Tris, pH 7.5; 0.1 mM EDTA) into the cytoplasm of C57BL/6J embryos in accordance with standard procedures approved by the IACUC at the NYU School of Medicine. Female CD-1 mice (Charles River) were used as foster mothers. F0 mice were

474 genotyped and sequenced (Sanger sequencing) to identify mice homozygous for both loxP
475 insertions. Founders bearing loxP insertions were then backcrossed at least one time to wild-
476 type C57BL/6J mice generating the *Vipr2*$^{fl/fl}$ mice. For the generation of ILC3$^{\Delta Vipr2}$ mice, *Vipr2*$^{fl/fl}$
477 mice were crossed with *Rorc*^{Cre} mice for the generation of *Rorc*^{Cre} *Vipr2*$^{fl/fl}$ and *Rorc*^{Cre} *Vipr2*$^{+/+}$
478 littermates.
479
480 *VIPen activation/inhibition using DREADDs*
481 To perform chemogenetic activation or inhibition of VIPen, we bred *VIP*$^{IRES\text{-}Cre}$ homozygous
482 mice to *hM3Dq*$^{fl\text{-}stop\text{-}fl}$ mice (DREADD for activation) or *hM4Di*$^{fl\text{-}stop\text{-}fl}$ mice (DREADD for
483 inhibition), generating *VIP*$^{IRES\text{-}Cre}$*hM3Dq*$^{fl\text{-}stop\text{-}fl}$ (VIPen activation) and *VIP*$^{IRES\text{-}Cre}$ *hM3Dq*$^{fl\text{-}stop\text{-}}$
484 ^{fl}*hM4Di*$^{fl\text{-}stop\text{-}fl}$ mice (VIPen inhibition). To perform 24h activation of the DREADDs, mice were
485 treated with Clozapine-N-Oxide (CNO, 1mg/Kg intraperitoneally, TOCRIS) each 12h. Our pilot
486 experiments in C57BL/6 mice (data not shown) revealed that at these dose CNO treatment
487 does not affect ILC3 function. To perform activation of the DREADDs during *Citrobacter*
488 *rodentium* infection, mice were treated daily with CNO (1mg/Kg, intraperitoneally) from day 1 to
489 day 4 after infection.
490
491 *Food restriction protocol*
492 For a period of two weeks, food was made available to mice only for 12h per daily cycle. Mice
493 were kept in two different regimens: Dark-phase fed mice, with food being available between 6
494 PM – 6AM (ZT 12->ZT 0); and light-phase fed, with food being available between 6 AM – 6PM
495 (ZT 0->ZT 12). To avoid littering, at the beginning of the fasting period of each regimen, mice
496 were transferred to a clean cage containing alpha cellulose clean bedding

(Shepherd's™ALPHA-dri). Mice were provided with free access to water.

Gavage of Liquid Test Diet

Dry powder micro stabilized rodent liquid diet (Test Diet, LD 101) was blended (mechanical blender) vigorously for 30 seconds in saline (NaCl 0.9%) at 0.5g/mL. Mice were gavaged with 400ul of this solution using a polyurethane feeding tube (16ga x 38mm, FTPU-16-38-50, INSTECH) every 45 min for 6 h.

Generation of bone marrow VIPR2$^{+/+}$/VIPR2$^{-/-}$ chimeric reconstituted mice

Bone marrow mononuclear cells were isolated from CD45.1 *VIPR2*$^{+/+}$ and CD45.2 (or CD45.1/2) *VIPR2*$^{-/-}$ mice by flushing the long bones. Red blood cells were lysed with ACK Lysing Buffer and the remaining cells were resuspended in PBS for injection in at a 1:1 ratio (WT:VIPR2 KO). 4×10^6 cells were injected intravenously into 6 week old CD45.1/2 (CD45.2) mice that were irradiated 4h before reconstitution using 1000 rads/mouse (2x500rads, at an interval of 3h, at X-RAD 320 X-Ray Irradiator). To deplete intestinal ILC3, one day after the bone marrow transfer, mice were treated with InVivoMAb anti-mouse Thy1.2 (200ug/mice for 4 consecutive days, Clone 30H12, BioXCell). Experiments were performed 6-7 weeks after the last treatment with α-Thy1.2.

Radioactively labeled triglyceride absorption assay

Plasma ^{3}H-CPM (counts per minute) was measured 1-4h after gavage with ^{3}H-Triolein–containing lipid[34]. Briefly, mice were injected with poloxamer 407 (1g/Kg, i.p., Sigma, #16758). After 30 minutes, mice were gavaged with a mixture of 2μCi ^{3}H-Triolein in

200ul of 20% intralipid oil emulsion. Blood samples were collected and diluted in Liquid Scintillation Counting cocktail (Ultima Gold) and measured using a Scintillation counter (Beta Counter MicroBeta^2 System, Perkin Elmer).

IL-22 in vivo Blockade

For experiments with IL-22 blockade, mice were injected with monoclonal α-IL-22 (Clone 8E11, 250μg/mouse, generously provided by Tangsheng Yi, Genentech), 12 hours before sample collection. Control groups received mIgG1 (inVivoMAb, BioXCell).

C. rodentium mediated colon inflammation

C. rodentium strain DBS100 (ATCC51459; American Type Culture Collection) was grown at 37°C in LB broth to OD600 reading between 0.5 and 0.7. *VIP*$^{IRES\text{-}Cre}$*hM3Dq*$^{fl\text{-}stop\text{-}fl}$ (VIPen activation) and C57BL/6 mice were inoculated with 200 µl of a bacterial suspension (2×10^9 CFU) by oral gavage. *VIP*$^{IRES\text{-}Cre}$ *hM3Dq*$^{fl\text{-}stop\text{-}fl}$*hM4Di*$^{fl\text{-}stop\text{-}fl}$ mice (VIPen inhibition) were inoculated with 200 µl of a bacterial suspension (4×10^{10} CFU) by oral gavage. For DREADD experiments, CNO treatment started at 1 day post-infection (d.p.i.) until 4 d.p.i. Mice were followed the next 12 days post-infection (d.p.i.) to measure survival rate. At 9 d.p.i. fecal pellets were collected and the mice dissected to harvest spleen and liver. Samples were weighted and minced on sterile deionized water with Triton 0.1% and filtered on a 70μm cell strainer. The filtered samples were used to measure *C. rodentium* burden with serial dilutions (triplicates) on MacConkey agar plates.

Immunofluorescence and Confocal Microscopy

Small intestine from SFB^{+} *Rorc*(γt)$^{EGFP/+}$ mice were Swiss-rolled, fixed for 4h in 4% paraformaldehyde, incubated overnight in 30% sucrose at 4^{o}C, and frozen in embedding medium for frozen specimens (O.C.T, Tissue-Tek, Sakura). Tissue was cut into 30-70 µM sections, blocked in PBST 0.5% (0.5% Triton X-100, 10% normal donkey serum) for 1 h, and incubated overnight using a combination of 3 of the following antibodies for 1 h: α-Vasoactive Intestinal Peptide (1:1000, rabbit polyclonal, 20077, Immunostar), α-Tyrosine Hydroxilase (1:50, rabbit polyclonal, AB152, Millipore), α-Substance P (1:3000, rabbit polyclonal, 20064 Immunostar), α-GFP Alexa Fluor 488 (1:500, clone: FM264G, Biolegend), α-TCRβ Brilliant Violet 421 (1:50, Biolegend), α-β-3-Tubulin Alexa Fluor 594 (1:500, clone:AA10, Biolegend). Tissue was washed and when needed incubated with secondary fluorescently labeled antibodies (Donkey Anti-Rabbit Pacific Blue or Alexa Fluor 647) for 2h before nuclear staining with Draq-7 (R&D Systems) or 4′,6-diamidino-2-phenylindole (DAPI, ThermoFisher). Images were acquired using a Zeiss LSM 710 confocal (Carl Zeiss). The imaging data were processed and analyzed using Image J software (NIH, Bethesda, MD). Imaris software version 9.0.1 (Bitplane; Oxford Instruments) was used to generated reconstructed 3D images.

Isolation of Lamina Propria Lymphocytes (LPLs) from the small intestine

Whole small intestine or the ileum (distal 14cm of the small intestine) was dissected from mice. Mesenteric fat tissue and Peyer's patches were carefully removed from these tissues. Intestinal tissue was opened and extensively cleaned of fecal matter. Following, this tissue was sequentially treated with HBSS 1X (1 mM DTT) at 37°C for 10 min with gentle shaking (200rpm), and twice with 5 mM EDTA at 37°C for 10 min to remove epithelial cells. The EDTA fraction (epithelial cell-enriched) was filtered, centrifuged and suspended in Trizol for further

RNA isolation. The remaining tissue was then minced with a scissor and dissociated in RPMI containing 10% FBS, Dispase (0.05 U/ml; Worthington), collagenase (1 mg/ml collagenase II; Roche) and DNase I (100 µg/ml; Sigma) at constant shaking at 37°C for 45 min (175rpm). The digested tissue was then filtered through a 70µm strainer to remove large debris. Viable Lamina Propria Lymphocytes (LPLs) were collected at the interface of a 40%/80% Percoll/RPMI gradient (GE Healthcare).

ILC3 in vitro cell culture

CCR6^{+} and CCR6^{neg} ILC3 (DAPI^{neg}CD3^{neg}CD11c^{neg}CD14^{neg}CD19^{neg}TCRβ^{neg}TCRγ^{neg}NK1.1^{neg}KLRG1^{neg}CD127^{+}CD90.2^{+}) were isolated from small intestine LPLs of C57BL/6 mice using the ARIA II FACS Sorter (BD Biosciences). ILC3 were cultured at 37°C in flat bottom 96 well plates (10^4 cells/well) in RPMI supplemented with 10% heat-inactivated FBS (Hyclone), 50 U penicillin-streptomycin (Hyclone), 2 mM glutamine (Hyclone), 10mM HEPES (Hyclone), 1mM sodium pyruvate (Hyclone) and 50 µM β-mercaptoethanol (Gibco). ILC3 were stimulated with IL-23 (100pg/mL, R&D systems) and/or VIPR2 ligands (BAY-559837: 1-100nM, and VIP: 1nM, TOCRIS) for 16h (37°C), washed, incubated in complete media in the presence of Golgi Plug (BD Bioscience) for 4h (37°C), and stained for membrane extracellular markers in Staining Buffer (PBS FBS2% EDTA 5mM) and for intracellular markers using Cytofix/Cytoperm buffer set following manufacturer's protocol (BD Biosciences). Acquisition of cytometric parameters was performed on an LSRII (BD Biosciences). All data were analyzed using FlowJo Software Version 10 (Tree Star).

589 *Antibodies for intracellular staining and flow cytometry*

590 Live/dead fixable blue (ThermoFisher) or DAPI (ThermoFisher) were used to exclude dead
591 cells. The following monoclonal antibodies were purchased from eBiosciences, BD
592 Pharmingen or BioLegend: CD3, CD45.1, CD45.2, TCRβ, CD11c, CD14, CD19, TCRβ, TCRγ,
593 NK1.1, CD127, CD90.2, CCR6, Sca-1 and IL-22. For cytokine analysis, cells were incubated
594 for 4 hours at 37C in RPMI with 10% FBS and GolgiPlug (BD). Cells were stained for surface
595 markers before fixation and permeabilization, and then subjected to intracellular cytokine
596 staining for IL-22 according to the manufacturer's protocol (Cytofix/Cytoperm buffer set from
597 BD Biosciences). Flow cytometric analysis was performed on an LSR II (BD Biosciences) or an
598 Aria II (BD Biosciences) and analyzed using FlowJo software version 10 (Tree Star).
599
600 *Blood collection*
601 Peripheral and portal vein blood were collected under general anesthesia (Ketamine
602 100mg/Kg, Xylazine 15mg/Kg). Peripheral blood was collected through orbital venous plexus
603 bleeding with a glass capillary in a tube containing EDTA (25mM) as an anticoagulant. Plasma
604 was collected after centrifugation of the collected sample and frozen until processing. Surgery
605 was performed to collect blood from the portal vein, which drains the gastrointestinal tract.
606 Briefly, after laparotomy, the portal vein was localized and the blood was collected with a
607 syringe. Portal vein blood was processed following the same protocol above for peripheral
608 blood.
609
610 *Tissue processing for ELISA*
611 Distal Ileum (6 cm from the ileal-cecal junction) or the Large intestine (Cecum + 3 cm of the

proximal colon) were collected and extensively washed to clean out fecal matter. The samples were weighed and, using a tissue homogenizer, extracted in PBS Tween 0.1% (with protease inhibitor) and centrifuged to remove tissue debris. The supernatant was frozen until measurement of VIP concentrations in the tissue.

ELISA for Vasoactive Intestinal Peptide

VIP content was measured in the blood plasma or homogenized tissue following manufacturer's recommendations (EIAM-VIP-1, RayBiotech).

Measurement of plasma concentration of triglycerides

Peripheral blood was collected as described above and plasma was used to quantify triglyceride concentrations following manufacturer's recommendations (Sigma-Aldrich, MAK266).

Scanning Electron Microscopy

Scanning Electron Microscopy was performed on 1-1.5 cm pieces from terminal ileum (2cm above the ileal-cecal junction). Intestine was cut open and washed to remove fecal matter, pinned in dental wax and fixed for 2h with a 0.1M sodium cacodylate buffer (CB, pH 7.4) containing 2.5% glutaraldehyde and 2% paraformaldehyde. Samples were post fixed in 1% OsO4 for 2 hours, dehydrated in ethanol, and critical point dried using Tousimis autosamdsri 931 (Rockwille, MD). The dried intestines were put on SEM stabs, sputter coated with gold/palladium by DESK V TSC HP Denton Vacuum (Moorestown, NJ), and images were taken on random locations in the tissue by Zeiss

635 Gemini300 FESEM using secondary electron mode at 5kv. For quantification of SFB
636 length, random fields were selected for measurement using Image J.
637
638 *RNA extraction from intestinal epithelial cells and RT-qPCR*
639 TRNA isolation of ileal epithelial cells was performed using TRIzol following
640 manufacter's instructions (Invitrogen) followed by DNase I (Qiagen) treatment and
641 cleanup with RNeasy MinElute kit (Qiagen) following manufacturer protocols. cDNA was
642 generated using SuperScriptTM IV First-Strand Synthesis System (ThermoFisher).
643 Gene-specific primers spanning exons were used: *Rps17* (F:'5-cgccattatccccagcaag-3'/
644 R:'5-tgtcgggatccacctcaatg-3'), *RegIIIγ* (F:'5-tctgcaagacagacaagatgct-3'/ R:'5-
645 ggggcatctttcttggcaac-3'), *Fabp2* (F:'5-gtctagcagacggaacggag-3'/R:'5-
646 ctccttcatatgtgtaggtctgga-3'), *Cd36* (F:'5-tggccttacttgggattgg-3'/R:'5-
647 ccagtgtatatgtaggctcatcca-3'). Quantitative PCR was performed using the Hot Start-IT
648 SYBRGreen (Affymetrix) on the Roche real-time PCR system (Roche 480). Values were
649 normalized to *Rps17* gene for each sample.
650
651 *Data processing of public available RNA-seq*
652 DESeq2-normalized gene quantification and differential expression analysis were downloaded
653 from GSE116092[16]. Raw counts were downloaded from GSE127267 (ImmGen ULI RNA-seq
654 data)[17] and differential expression analysis was performed using DESeq2. Normalized counts
655 were used for downstream analysis. A cutoff was made based on the normalized counts of a
656 non-expressed gene (*Foxp3*) (GSE116092, cut-off $\leq$ 9 and for GSE127267, cut off <25). A list
657 with neural-associated related genes list was made from 3 databases - KEGG, Amigo2, and

G3Cdb. For the KEGG list, all genes involved in the following pathways were included: Glutamatergic synapse, GABAergic synapse, Cholinergic synapse, Dopaminergic synapse, Serotonergic synapse, Long-term potentiation, Long-term depression, Retrograde endocannabinoid signaling, Synaptic vesicle cycle, Neurotrophin signaling pathway, Axon guidance, Circadian rhythm, Circadian entrainment, Neuroactive ligand-receptor interaction, Cell adhesion molecules (CAMs), and cAMP signaling pathway. The Amigo2 list included genes from the following GO classes - vasoactive intestinal polypeptide receptor activity, G protein-coupled peptide receptor activity, nervous system development, positive regulation of neuron projection development, cerebellum development, neuron projection development, anchored component of postsynaptic membrane, and anchored component of presynaptic membrane. The G2Cdb list was formed with genes from the following lists -L00000001, L00000008, L00000060, L00000062, L00000070 and L00000072. GO term analysis of GSE116092[16] was done using g:Profiler. For heat maps, genes were considered differentially expressed with FDR < 0.01 and log2 fold change $\geq$ 2.

Statistical analysis

Unpaired two-sided *t-test*, paired two-sided *t-test,* one-way ANOVA with multiple comparisons with Bonferroni correction, two-way ANOVA with multiple comparisons and Bonferroni correction, Mann-Whitney test, Mantel Cox test (for survival curves), were performed to compare the results using GraphPad Software Version 8 (GraphPad Software). No samples were excluded from analysis. We treated less than 0.05 p value as significant. $*P < 0.05$, $** P < 0.01$, $*** P < 0.001$, and $**** P < 0.0001$. Details regarding number of replicates and the definition of center/error bars can be found in figure legends.

EXTENDED DATA FIGURE LEGENDS

Extended Data Figure 1. Enrichment of transcripts related to nervous system/neural functions and development in CCR6^{+} ILC3. a, Volcano-plot of differentially expressed genes between CCR6^{+} ILC3 and CCR6^{neg} ILC3 isolated from the small intestine of C57BL/6 mice GSE116092[16]. Green: Neurotransmitter/neuropeptide receptors, Blue: genes related to nervous system development/axonal guidance and contact. **b,** Top 10 Gene-Ontology terms from a comparison between subtypes of ILC3 showing enrichment of transcripts related to neuron differentiation and generation in CCR6^{+} ILC3 when compared to CCR6^{neg} ILC3. Green: Neurotransmitter receptors, Blue: genes related to nervous system development/axonal guidance and contact. **c,** Vocano-plot of differentially expressed genes between CCR6^{+} ILC3 (enriched in cryptopatches and ILFs[35]) and NKp46^{+} ILC3 (low presence in CPs and ILFs[36]) (GSE127267[17]).

Extended Data Figure 2. Neurochemical code of the cryptopatch-associated enteric neurons in the small intestine lamina propria. a-c, Representative immunofluorescence images of different subtypes of lamina propria neuronal projections of enteric neurons in the small intestine of *Rorc(γt)*$^{EGFP/+}$ mice. **(a)** Substance P (green) does not represent the neuronal projections (βIII-Tubulin, red) localized inside CPs/ILFs (cluster of GFP^{+} cells, blue) in the lamina propria. **(b)** Tyrosine hydroxylase^{+} neurons (green) are in close proximity but are not the CP-associated neuronal projections (βIII-Tubulin, red) localized inside CPs/ILFs (cluster of

GFP$^+$ cells, blue) in the lamina propria. **(c)** Vasoactive Intestinal Peptide$^+$ (green) neurons (βIII-Tubulin, red) are in close proximity and interacting with ILC3 (GFP$^+$, blue) in CPs/ILFs.

Extended Data Figure 3. Cryptopatch-associated enteric neurons are also localized in the large intestine (colon) lamina propria. a, b Representative immunofluorescence images of lamina propria neuronal projections of enteric neurons in the large intestine of *Rorc(γt)*$^{EGFP/+}$ mice. **(a)** Cluster of ILC3 (GFP$^+$ cells, green) in close proximity of neuronal projections (βIII-Tubulin, red) of the enteric neurons in the colon lamina propria. **(b)** Cluster of ILC3 (GFP$^+$ cells, blue) in close proximity of neuronal projections (βIII-Tubulin, red) of the Vasoactive Intestinal Peptide$^+$ enteric neurons (VIPen, green) in the colon lamina propria.

Extended Data Figure 4. VIP agonist inhibits *in vitro* IL-22 production by CCR6$^+$ ILC3. a, FACS plot showing gating strategy for identification and isolation of CCR6$^+$ or CCR6^{neg} ILC3 (DAPI^{neg}Lin^{neg} CD127$^+$ CD90.2$^+$). **b, c,** *In vitro* activation of VIPR2 alone does not induce cytokine production or activation of CCR6$^+$ ILC3. Representative FACS plots **(b)** and summary **(c)** for surface Sca-1 expression and intracellular IL-22 in small intestine lamina propria CCR6$^+$ ILC3 stimulated *in vitro* for 12h with IL-23 (100pg/mL) or different concentrations of the VIPR2 ligand BAY-559837. N= 3, ***P*=< 0.01 (One-way ANOVA). Data are representative of two independent experiments. **d,** *In vitro* activation of VIPR2 does not modulate IL-23-induced Sca-1 expression on CCR6$^+$ ILC3. Summary of Sca-1 expression in small intestine lamina propria CCR6$^+$ ILC3 stimulated *in vitro* for 12h with IL-23 (100pg/mL) or different

concentrations of the VIPR2 ligands BAY-559837 and VIP (N= 3). **e, f,** *In vitro* VIPR2 activation does not affect IL-23-induced IL-22 production by CCR6^{neg} ILC3. Representative FACS plots **(e)** and summaries **(f)** of surface Sca-1 expression and intracellular IL-22 in small intestine lamina propria CCR6^{neg} ILC3 stimulated *in vitro f*or 12h with IL-23 (100pg/mL) with/without combination with VIPR2 ligand BAY-559837 (1nM) (N= 3). Data are representative of two independent experiments.

Extended Data Figure 5. VIPR2 is required for *in vivo* inhibition of IL-22 production by CCR6^{+} ILC3. a, b, Mixed bone marrow chimeras, showing **(a)** no difference in frequency and ratio of WT (*Vipr2*$^{+/+}$) vs VIPR2 KO (*Vipr2*$^{-/-}$) CCR6^{+}ILC3 in the ileum of mice receiving equal number of cells (N=17 mice, combined from 2 independent experiments) and **(b)** VIPR2-dependent inhibition of IL-22 production in WT (*Vipr2*$^{+/+}$, CD45.1) versus VIPR2 KO (*Vipr2*$^{-/-}$, CD45.2) CCR6^{+} ILC3 in the ileum of chimeric mice. N=11, ****P<0.0001 (*paired t-test*). Data are representative of two independent experiments. **c, d,** Inactivation of *Vipr2* in ILC3 (ILC3$^{\Delta Vipr2)}$ does not affect **(c)** frequency or **(d)** number of CCR6^{+} ILC3 in the mouse ileum. WT: N=8; ILC3$^{\Delta ILC3.}$: N=6. **e, f,** Representative FACS plot (C) and summaries (D) indicating frequency of IL-22 expression in CCR6^{+} ILC3 from the ileum of WT and ILC3$^{\Delta Vipr2}$ mice. WT: N=8; ILC3$^{\Delta Vipr2}$: N=6, ***P<0.001 (*t-test*),

Extended Data Figure 6. VIPen regulate host resistance to enteropathogenic *Citrobacter rodentium*. **a,** Normalized *Vip* mRNA expression in the large intestine (cecum and proximal colon) of C57BL/6 mice at different time points after oral infection with *Citrobacter rodentium* ($2x10^9$ CFU). **Day** 0: N=4; Days 2, 4 and 9: N=6. **P*<0.05 compared to day 0 (one-way ANOVA)**. b, c,** Increased VIP activity in the gastrointestinal tract but not systemically in mice infected with *C. rodentium.* Concentrations of VIP in plasma from the (**b**) hepatic portal vein, which drains the gastrointestinal tract, and (**c**) peripheral blood of mice at different time points after intragastric administration of vehicle or *C. rodentium* ($2x10^9$ CFU). d.p.i: days post-intragastric infection with *C. rodentium*. N= 3/group, **P*<0.05 (*t-test*). **d, e** Infectious burden in feces of (**d**) $Vip^{IRES\text{-}Cre}hM3Dq^{fl\text{-}stop\text{-}fl/+}$ (activating DREADD) and (**e**) $Vip^{IRES\text{-}Cre}hM4Di^{fl\text{-}stop\text{-}fl/+}$ (inhibitory DREADD) mice treated with vehicle or CNO (1mg/Kg, daily, 1-4 days post-intragastric infection with $2x10^9$ CFU for activating and $4x10^{10}$ CFU for inhibitory DREADD mice). Log_{10} Colony Forming Units (CFU) of *C. rodentium* 9 days post-oral innoculation (9 d.p.i.). Data representative of two independent experiments. Activating DREADD mice: Vehicle: n=11, CNO: n=9. Inhibitory DREADD mice: Vehicle: n=8, CNO: n=7**,** **P*=0.0009 (Mann-Whitney test). **f, g,** Exogenous treatment with recombinant murine IL-22 (rmIL-22, 250μg/mouse/day) protects against increase in **(f)** mortality and **(g)** bacterial dissemination induced by VIPen activation of $Vip^{IRES\text{-}Cre}hM3Dq^{fl\text{-}stop\text{-}fl/+}$ mice. ***P=0.0321 (Mantel Cox test,* survival); ***P*=0.0022 *(*Mann-Whitney test).

Extended Data Figure 7. Feeding controls intestinal VIP release, growth of epithelium-

associated segmented filamentous bacteria, and lipid absorption. a, Measurement of concentration of VIP in the ileum reveals higher amounts during dark-phase (feeding period, ZT12-ZT0) than in the light-phase (resting period, ZT0-ZT12). N=4, representative of two independent experiments. **b,** Concentrations of VIP in plasma isolated from hepatic portal vein blood of mice fed or fasted for 6 h. Blood samples were collected at two different time-points, during the light-phase period (ZT 6, 12PM) and the dark-phase period (ZT 18, 12AM). N=4, **P*<0.05*;* ***P*<0.01 (*t-test*). **c,** Concentrations of VIP in plasma isolated from the peripheral blood of mice. Blood samples were collected at two time-points, during the light-phase period (ZT 6, 12PM) and the dark-phase period (ZT 18, 12AM). N=4. **d,** Representative SEM Image (1K and 3K magnification) showing epithelial-attached SFB in the ileum of mice 12 h after feeding (long filaments) or fasting (short-filaments, "stubbles") at ZT 0. **e,** SFB lengths at different time points during the day in mice that had been fed for two weeks during the dark-phase (ZT12-> ZT0) or during the light-phase (ZT0-> ZT12). **f, g,** Plasma ^{3}H CPM (counts per minute) in mice fed or fasted for 12h during the light-phase (ZT 0 – ZT 12, red and green circles) or during the dark-phase (ZT 12 – ZT 0, blue and black circles) and then gavaged with ^{3}H-triolein were sampled at different times (**f**) and the AUC during 4h was determined for individual mice from each group (**g**). AUC: Area under the curve per mL of plasma. N=4 mice per group, **P* < 0.05 and *****P* < 0.001 (two-way ANOVA).

Supplementary Videos

Supplementary Video 1. 3D software reconstruction of Figure 1b showing the small intestine of *Rorc(γt)*$^{EGFP/+}$ mice with a cluster of intestinal ILC3 (cryptopatch) in close proximity to enteric neurons. Pan-neuronal marker: β3-tubulin^{+} (red), ILC3: GFP^{+} (green).

Supplementary Video 2. 3D software reconstruction of Figure 1c from the small intestine of *Rorc(γt)*$^{EGFP/+}$ mice showing ILC3 in the cryptopatch in close proximity to enteric neurons in the small intestine lamina propria. Pan-neuronal marker: β3-tubulin^{+} (red), ILC3: GFP^{+} (green).

Supplementary References

32. Wang H, Yang H, Shivalila CS, et al. One-step generation of mice carrying mutations in multiple genes by CRISPR/Cas-mediated genome engineering. *Cell.* 2013;153(4):910-918.
33. Yang H, Wang H, Jaenisch R. Generating genetically modified mice using CRISPR/Cas-mediated genome engineering. *Nat Protoc.* 2014;9(8):1956-1968.
34. Zhang F, Zarkada G, Han J, et al. Lacteal junction zippering protects against diet-induced obesity. *Science.* 2018;361(6402):599-603.
35. Lugering A, Ross M, Sieker M, et al. CCR6 identifies lymphoid tissue inducer cells within cryptopatches. *Clin Exp Immunol.* 2010;160(3):440-449.
36. Reynders A, Yessaad N, Vu Manh TP, et al. Identity, regulation and in vivo function of gut NKp46+RORgammat+ and NKp46+RORgammat- lymphoid cells. *EMBO J.* 2011;30(14):2934-2947.

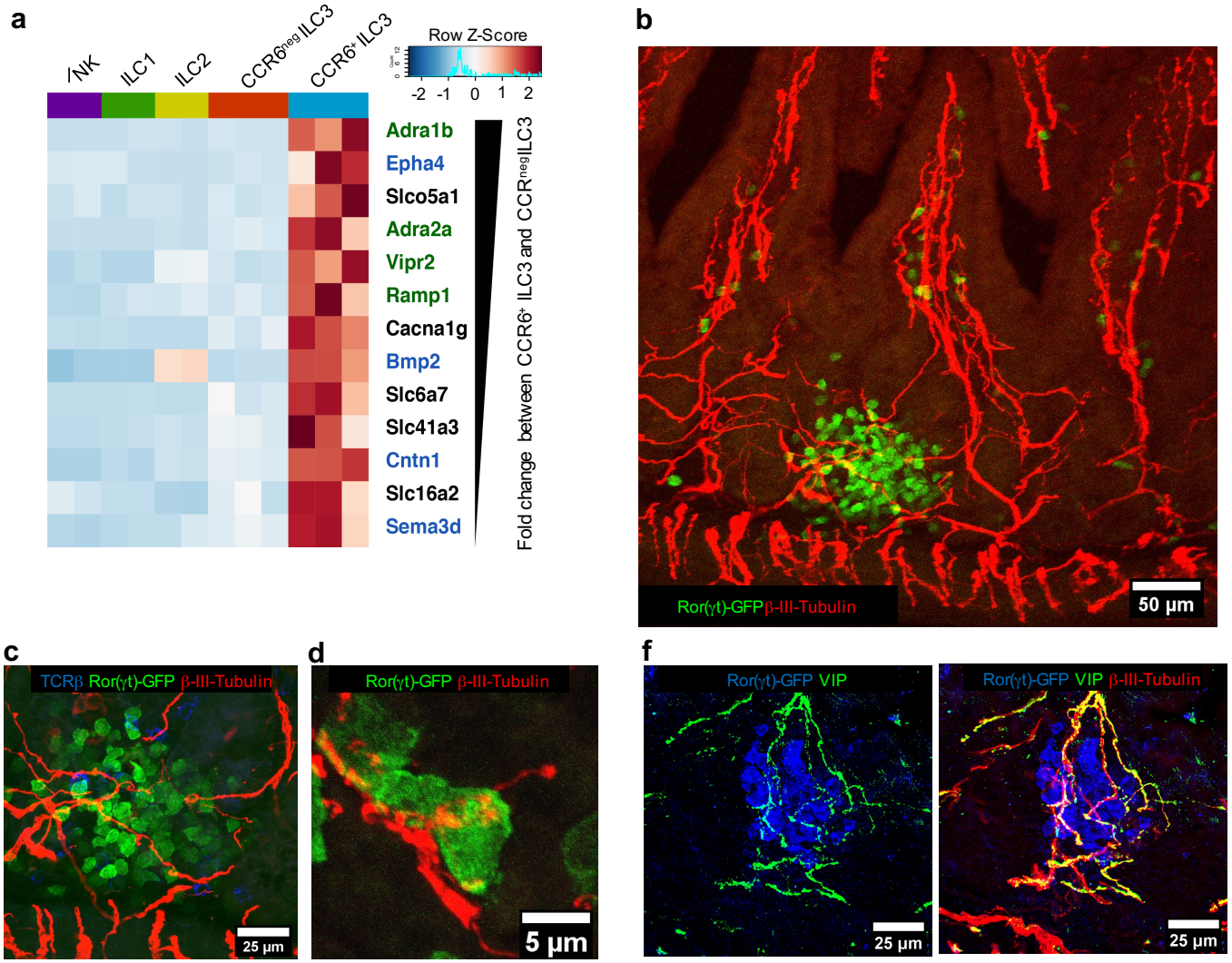

Figure 1. Processes of VIP-producing enteric neurons are in close proximity to *Vipr2*-expressing ILC3 within cryptopatches. a, Heatmap of differentially expressed neural-related genes between intestinal CCR6^{+} ILC3 and CCR6^{neg} ILC3 (Fold change $\geq$ 2, *p-value <0.05,* GSE116092). Color scale is based on normalized read counts. Genes are listed on the right hand margin ranked based on the relative fold change, and color coded: Green: Neurotransmitter/neuropeptide receptors, Blue: genes related to nervous system development/axonal guidance and contact. Expression in other ILC subsets is included for comparison. **b-d,** Representative confocal images from the small intestine of *Rorc(γt)*$^{EGFP/+}$ mice show clusters of intestinal ILC3 (cryptopatch) in close proximity to enteric neurons in the small intestine lamina propria (see supplementary video 1 and 2). Pan-neuronal marker: β3-tubulin^{+} (red), ILC3: GFP^{+}TCRβ^{neg} (green and blue, respectively). n=4 mice, 45 ILC3 clusters. **e, f,** Neurochemical code of cryptopatch-associated enteric neurons. (**e**) Representative confocal images from the small intestine of *Rorc(γt)*$^{EGFP/+}$ mice show cryptopatch-associated enteric neurons are positive for VIP. Neurons: β3-tubulin^{+} (red), VIP^{+} (green); ILC3: GFP^{+} (blue).

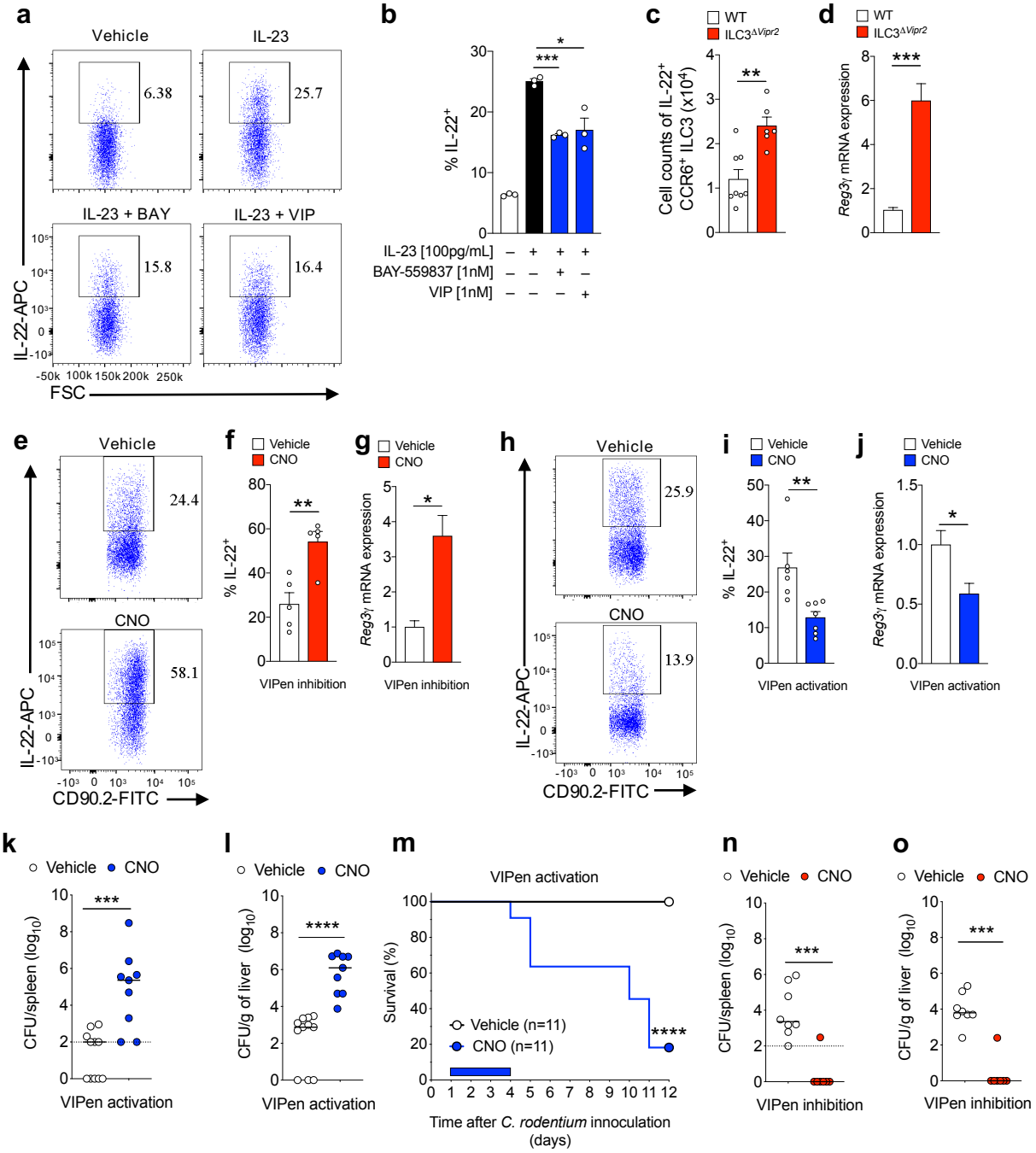

Figure 2. VIPen promote reduction of mucosal barrier function by VIPR2-dependent inhibition of CCR6⁺ ILC3. a, b, Representative FACS plot (**a**) and summaries (**b**) indicating IL-22 expression in purified CCR6⁺ ILC3 after *in vitro* IL-23 stimulation with/without VIPR2 agonist ligands. BAY: BAY-559837, VIP: vasoactive intestinal peptide. **P*<0.05 and ****P*<0.001 (*t-test*). Data are representative of three independent experiments. **c,** Number of IL-22⁺ CCR6⁺ ILC3 present in the ileum of *Rorc*^{Cre} (WT) and *Rorc*^{Cre} *Vipr2*$^{fl/fl}$(ILC3$^{\Delta Vipr2}$).. ***P*<0.01 (*t-test*), WT: 8; ILC3$^{\Delta Vipr2}$: 6. **d,** Normalized epithelial *Reg3γ* mRNA from ileum of WT and ILC3$^{\Delta Vipr2}$ mice. ****P*<0.001 (*t-test*), WT: 5; ILC3$^{\Delta Vipr2}$: 5. **e-g,** Effect of VIPen inhibition on ILC3 and intestinal epithelial cells (IEC). Representative FACS plot (**e**) and summary (**f**) indicating IL-22 expression in CCR6⁺ ILC3 from the ileum of *Vip*$^{IRES\text{-}Cre}$*hM4Di*$^{fl\text{-}stop\text{-}fl/+}$ mice (DREADD for VIPen inhibition) 24h following treatment with vehicle or CNO (Clozapine-N-oxide, DREADD ligand). Vehicle: n=5, CNO: n=5. ***P*<0.01 (*t-test*). Data representative of three independent experiments. **g,** Normalized *Reg3γ* mRNA expression in IEC at 24h following treatment. Vehicle: n=3, CNO: n=3. **P*<0.05 (*t-test*). Data representative of two independent experiments. **h-j,** Effect of VIPen activation on ILC3 and IEC. Representative FACS plot (**h**) and summaries (**i**) indicating IL-22 expression in CCR6⁺ ILC3 from ileum of *Vip*$^{IRES\text{-}Cre}$*hM3Dq*$^{fl\text{-}stop\text{-}fl/+}$ (DREADD for VIPen activation) 24h following the treatment with vehicle or CNO.

Continuation Figure 2. Vehicle: 6, CNO: 7. ***P*<0.01 (*t-test*). **j,** Normalized epithelial *Reg3γ* mRNA at 24h following treatment with vehicle or CNO. Vehicle: 7, CNO: 6. **P*<0.05 (*t-test*). Data representative of three independent experiments. **k, l,** Dissemination of *C. rodentium* to the (**k**) spleen and (**l**) liver in $Vip^{IRES\text{-}Cre}hM3Dq^{fl\text{-}stop\text{-}fl/+}$ mice treated with vehicle or CNO (1mg/Kg, daily) for 4 days post-intragastric infection with $2x10^9$ CFU. Log_{10} Colony Forming Units (CFU) of *C. rodentium* 9 days post-oral innoculation (9 d.p.i.). Dotted line: limit of detection. ****P*=0.0009 and ****P<0.0001, (*Mann-Whitney test*). Vehicle: n=11 (Positive for *C. rodentium:* spleen: 6/11, liver: 8/11), CNO: n=9 (Positive for *C. rodentium:* spleen and liver: 9/9). Data representative of two independent experiments. **m,** Survival rates for *C. rodentium*-infected $Vip^{IRES\text{-}Cre}hM3Dq^{fl\text{-}stop\text{-}fl/+}$ mice treated with vehicle or CNO (1mg/Kg, daily, 1-4 d.p.i.: blue rectangle). Vehicle: n=11, CNO: n=11. Data representative of three independent experiments. *****P*<0.0001 *(Mantel-Cox test*). **n, o,** Bacterial dissemination to the (**n**) spleen and (**o**) liver of $Vip^{IRES\text{-}Cre}hM4Di^{fl\text{-}stop\text{-}fl/+}$ mice treated with vehicle or CNO (1mg/Kg, daily, 1-4 days post-intragastric infection with $4x10^{10}$ CFU of *C. rodentium*). Log_{10} CFU at 9 d.p.i. Dotted line: limit of detection. Vehicle: n=8 (Positive for *C. rodentium:* spleen: 8/8, liver: 8/8), CNO: n=7 (Positive for *C. rodentium:* spleen: 1/7, liver: 1/7). ****P*=0.0006 (spleen) and ****P*=0.0005 (liver) (*Mann-Whitney test*)**.** Data representative of two independent experiments.

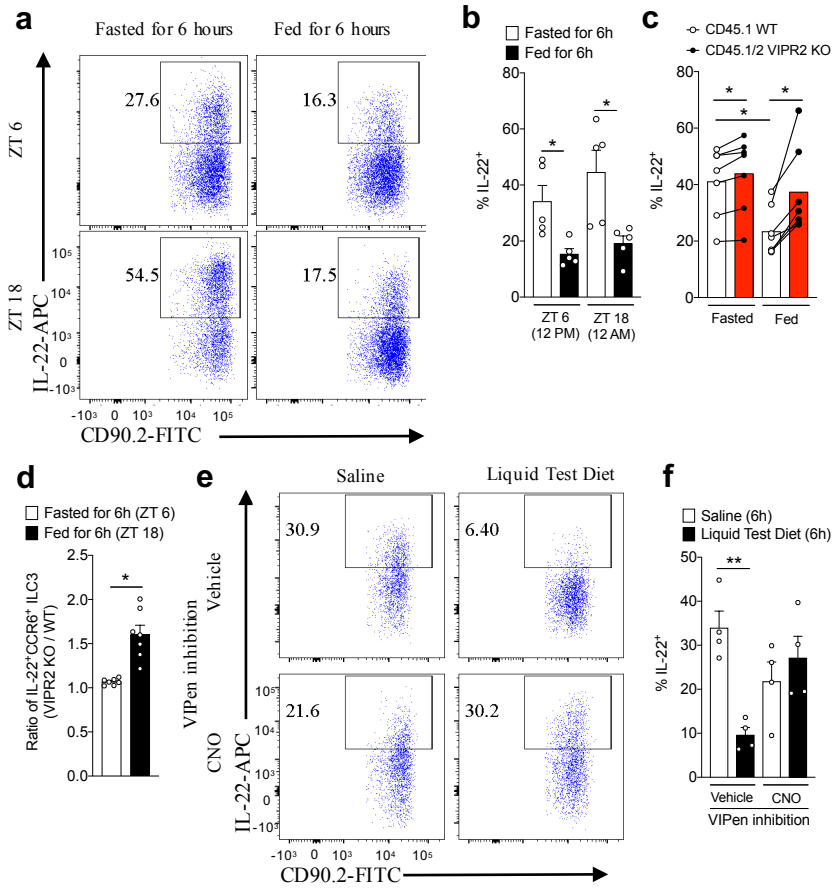

Figure 3. Feeding reduces IL-22 production by CCR6⁺ILC3 through activation of VIPen. a, b, Representative FACS plot (**a**) and summaries (**b**) indicating IL-22 expression among CCR6⁺ ILC3 from the ileum of mice 6h after feeding or fasting, at ZT6 and ZT18. N=5, **P*<0.05 (*t-test*). Data are representative of two independent experiments. **c,** IL-22 expression by CCR6⁺ ILC3 from the ileum of CD45.1 *Vipr2*$^{+/+}$:CD45.2 *Vipr2*$^{-/-}$ bone marrow chimeric mice 6h after fasting (fasted, ZT 6) and 6h after feeding (fed, ZT 18). n=7, **P*<0.05 (*paired t-test*). Data are representative of two independent experiments. **d,** Ratio of IL-22-expressing cells, relative to Figure 3c, among CCR6⁺ ILC3 from the ileum of CD45.1 *Vipr2*$^{+/+}$:CD45.2 *Vipr2*$^{-/-}$ bone marrow chimeric mice 6h after fasting (Fasted, ZT 6) and 6 hours after feeding (Fed, ZT 18). n=7, **P*<0.05 (*t-test*). **e, f,** Representative FACS plot (**e**) and summaries (**f**) indicating IL-22 expression in CCR6⁺ ILC3 from the ileum of *Vip*$^{IRES\text{-}Cre}$*hM4Di*$^{fl\text{-}stop\text{-}fl/+}$ mice (DREADD for VIPen inhibition). Mice were treated with vehicle or CNO (1mg/Kg) and 30 minutes later were fed by intragastric administration of saline (0.4 mL each 45 min, for 6 h) or Liquid Test Diet (500 mg/mL, 0.4mL each 45 minutes, for 6 h). N=4, ***P*<0.01 (*t-test*).

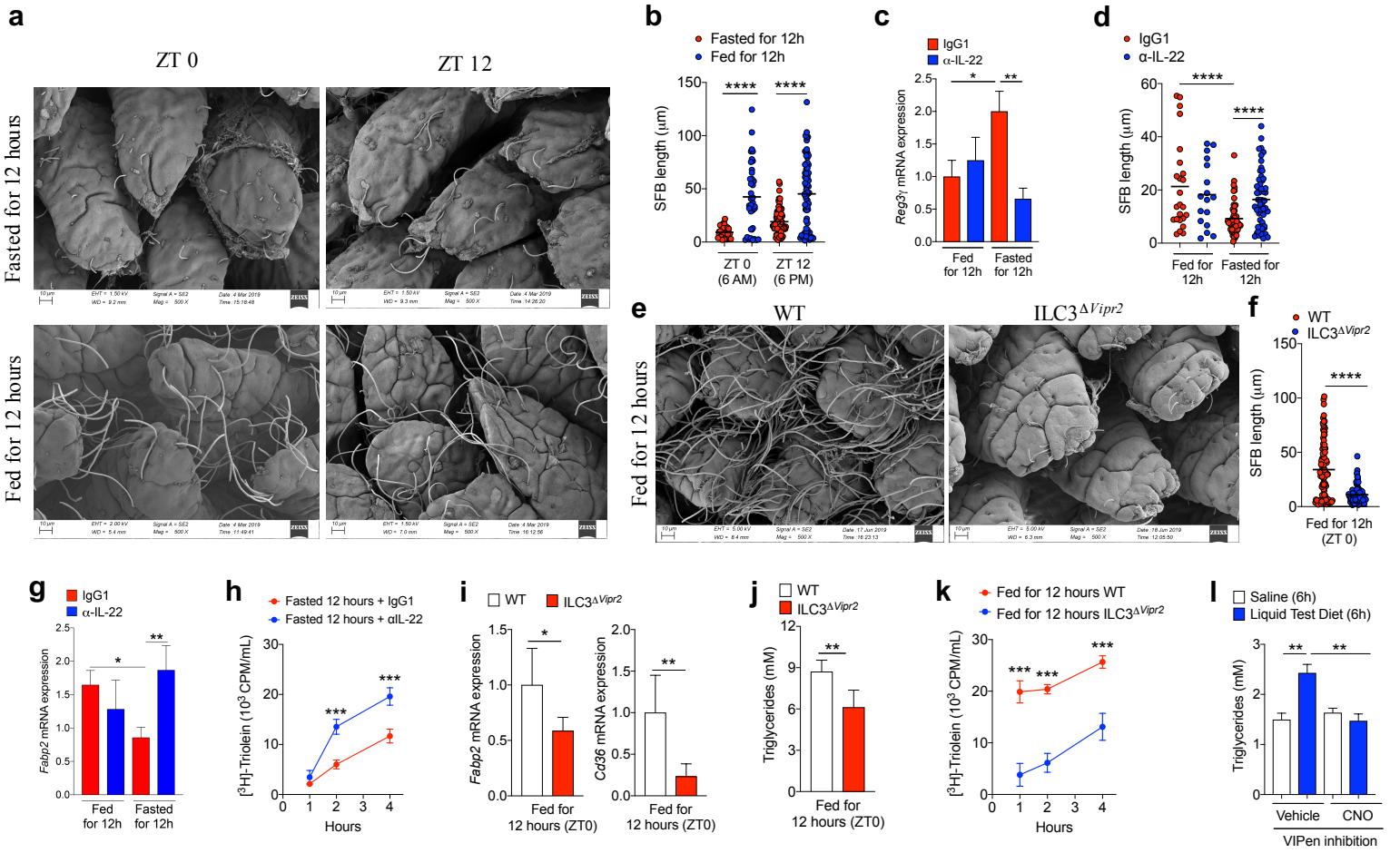

Figure 4. Dynamic regulation of commensal bacterial growth and lipid absorption by feeding-dependent VIP production . a, b, Representative scanning electron microscopy (SEM) images (**a**) of epithelium-associated commensal SFB in the ileum of mice 12h after fasting or feeding at the end of the dark-phase (ZT 0) and the light-phase (ZT 12) and (**b**) measurements of SFB filament lengths. N=3, ****P<0.001 (*t-test*). **c,** Normalized epithelial *Reg3γ* mRNA expression in the ileum of mice treated with IgG or α-IL-22 (10mg/Kg) during the feeding period (Fed for 12h: Treated from ZT 12->ZT 0) or during the fasting period (Fasted for 12h: Treated from ZT 0->ZT 12). Data pooled from 2 independent experiments: Fed IgG1: N=8, Fed α-IL-22: N=8, Fast IgG1: N=8, Fed α-IL-22: N=7, *P<0.05 and **P<0.01 (*t-test*). **d,** SFB length in the ileum of mice treated with IgG or α-IL-22 (10mg/Kg) during the feeding period (Fed for 12h: ZT 12->ZT 0) or during the fasting period (Fast for 12h: ZT 0->ZT 12). N= 3, ****P<0.001 (*t-test*). **e,f,** Representative **(e)** SEM images of epithelium-associated SFB in the ileum of WT and ILC3$^{\Delta Vipr2}$ mice fed for 12h and **(f)** measurement of bacterial filament lengths. N= 3, ****P<0.001 (*t-test*). **g,** Normalized epithelial mRNA expression of *Fabp2* in the ileum of mice treated with IgG or α-IL-22 (10mg/Kg) during the fasting period (Fasted for 12h: Treated from ZT 0->ZT 12). Data pooled from 2 independent experiments: Fed IgG1: N=8, Fed α-IL-22: N=8, Fast IgG1: N=8, Fed α-IL-22: N=7. *P<0.05 and **P<0.01 (*t-test*). **h,** Plasma ^{3}H CPM (counts per minute) in 12h fasted mice after gavage with ^{3}H-triolein (1uCi/mice in 200ul of 20% Intralipid). Mice were treated with IgG or α-IL-22 (10mg/Kg) during the fasting period (Fasted for 12h: Treated from ZT 0->ZT 12). Data representative of 2 independent experiments. N=4, ***P<0.001 (*two-way ANOVA*). **i, j,** Normalized epithelial mRNA expression of *Fabp2* and *Cd36* (**i**) and plasma triglyceride content (**j**) in 12h fed WT (N=5) and ILC3$^{\Delta Vipr2}$ (N=4) mice**.** *P<0.05 and **P<0.01 (*t-test*). **k,** Plasma ^{3}H CPM in 12h fed WT (N=3) and ILC3$^{\Delta Vipr2}$ (N=3) mice after gavage with ^{3}H-triolein. ***P<0.001, (*two-way ANOVA*). **l,** Plasma triglyceride content in *Vip$^{IRES-Cre}$hM4Di$^{fl-stop-fl/+}$* mice (DREADD for VIPen inhibition) after gavage with Saline (0.4 mL/each 45 minutes, for 6 hours) or Liquid Test Diet (500 mg/mL, 0.4mL/each 45 minutes, for 6 hours). Vehicle: N=5, CNO: N=4. **P<0.01, (*t-test*).